IEEE Access
Multidisciplinary | Rapid Review | Open Access Journal

Received October 26, 2017, accepted December 16, 2017, date of publication December 21, 2017,
date of current version February 14, 2018.

Digital Object Identifier 10.1109/ACCESS.2017.2785809

Characteristic Mode Analysis of Complex Spoof Localized Surface Plasmon Resonators

ZHIXIA XU, (Student Member, IEEE), SHUNLI LI, (Member, IEEE), YANQUN LIU, (Student Member, IEEE), HONGXIN ZHAO, (Member, IEEE), AND XIAOXING YIN, (Member, IEEE)
State Key Laboratory of Millimeter Waves, Southeast University, Nanjing 210096, China

Corresponding author: Xiaoxing Yin (101010074@seu.edu.cn)

This work was supported by the National Natural Science Foundation of China under Grant 61427801, Grant 61771127, Grant U1536123, and Grant U1536124.

ABSTRACT In this paper, characteristic mode analysis (CMA) is originally applied to investigate complex spoof localized surface plasmon (LSP) resonators, including a traditional toroid spoof-LSP resonator, and three Fabry–Perot type spoof-LSP resonators with different boundary conditions: open, shorted, and reactive. Compared with three traditional analytical methods of spoof LSP: dispersion curve approximation, near-field measurement (NFM), and extinction cross-sectional simulation (ECSS), CMA has three main advantages: to provide an insight of intrinsic resonances independent of excitations, to provide eigencurrents distribution, and to track each resonant mode at the full frequency band even when many resonant modes coexist at a very narrow band. Resonant frequencies calculated by CMA match well with that obtained by NFM and ECSS, indicating the correctness of CMA method. Based on CMA, bandwidths and eigencurrents of different resonant modes are also presented. It is foreseeable that CMA could be further utilized in spoof-LSP designs for various applications.

INDEX TERMS Characteristic mode analysis, Fabry–Perot resonator, spoof localized surface plasmon, surface waves.

I. INTRODUCTION

Surface waves on corrugated metal surfaces have been discussed for many years [1]–[3]. Based on similar sub-wavelength structures, the concept of spoof surface plasmon polaritons (SSPPs) has been proposed to mimic optical surface plasmons (SPs) at microwave band and terahertz band, promoting the possibility of manipulating electromagnetic (EM) waves propagation, localization and radiation [4]–[10]. When SSPPs transmission lines are bent into a circle, SSPPs waves propagate forward and backward simultaneously to form standing waves and this kind of resonance is called as spoof localized surface plasmon (LSP). Recently, spoof-LSP on various structures have been discovered with complex response spectra: Pors *et al.* [11] investigated spoof-LSP on textured metal cylinder; Shen and Cui [12] reviewed spoof-LSP and some spoof-LSP sensors on planar metal structures; Gao *et al.* [13], [14] designed fan-shaped metal surfaces to support spoof-LSP as well as spoof-LSP transmission structures; Wu *et al.* [15] discussed characteristics of spoof-LSP on a textured closed surface with defeats; Huidobro *et al.* [16] proposed magnetic spoof-LSP. Commonly, the response spectra of spoof-LSP resonators are complex. Multiple spoof-LSP resonances with different levels of energy could be excited in the spectra. There are three traditional methods to analyze these complex spoof-LSP resonances: The first method is dispersion curve approximation (DCA). Resonant frequencies could be calculated when the dispersion curve is obtained [12], [13]. However, results are certain approximations because rectangle-shaped unit cells are used to represent fan-shaped unit cells in simulation that brings geometric deviation inevitably. The second method is near field measurement (NFM) [12], [14], [17]. It is convenient to obtain near-field (NF) response spectra by NFM but difficult to track spoof-LSP resonances at low frequency band because the NF probes are too small to detect low frequency signals. Moreover, the existence of NF probes brings distortion to field distribution and causes frequency shift due to the reactance of probes. The third method is extinction cross section simulation (ECSS) [18]–[22]. This method obtains far field response spectra under plane wave

excitations. However, field and eigencurrents distribution are distorted by plane wave excitations; moreover, the extinction cross section (ECS) of each mode varies greatly and the number of resonant peaks at spectra could be fewer than theoretical prediction as observed in [19]. More importantly, spectra obtained by both NFM and ECSS are superposition of responses from all modes; and it is hard to distinguish each resonant mode when multiple resonant modes are excited at a narrow band.

As mentioned before, complex spoof-LSP resonances have been analyzed and applied to the field of sensor designs; however, the development of analytical methods stands still with some disadvantages. Therefore, this paper is aimed at finding a powerful method to study spoof-LSP resonances. We regard characteristic mode analysis (CMA) as a potential candidate. CMA was first proposed by Garbacz and Turpin [23] to find a set of independent eigencurrents of an arbitrary metal structure under open boundary condition. Recently, CMA has been applied to various antenna problems such as, mutual coupling reduction [24], antenna platform designs [25], antenna array [26], metasurface antenna [27], and optical antennas [28]. Reviews on CMA can be found in [29] and [30]. CMA frees us of influence from feeding structures at the beginning of antenna designs and provides an insight on each natural resonant mode of a geometric structure. Since spoof-LSP resonances are also intrinsic resonances of structures, it is desirable to use CMA to calculate resonant frequencies, bandwidths, and eigencurrents of each resonant state without influence from excitations.

To vindicate the robustness of CMA in the field of spoof-LSP resonances, four complex spoof-LSP resonators are proposed and investigated by CMA respectively: a traditional toroid spoof-LSP resonator and three Fabry-Perot (F-P) type spoof-LSP resonators with various boundary conditions. It should be mentioned that the boundary condition of F-P type spoof-LSP resonators could be used as a controllable parameter to manipulate spoof-LSP resonances. However, researches about F-P type spoof-LSP resonators with complex boundary conditions have not been reported due to the disadvantages of traditional analytical methods listed before: it is difficult to conduct DCA due to the lack of precise reflection characteristics at terminals of F-P type resonators; when we conduct NFM, coupling between NF probes increases dramatically because the F-P type resonators are usually smaller than traditional toroid resonators; and when we conduct ECSS, radiation from terminals of F-P type resonators may influence observation of resonant peaks. Based on CMA, this paper investigates various complex resonant modes separately without the influence of excitations such as plane waves and NF probes.

The rest of this paper is organized as follows. Section II presents the mathematical background of CMA. Section III deduces a general spoof-LSP resonant condition and designs complex spoof-LSP resonators. Section IV presents CMA results and makes comparisons with results obtained by traditional methods. Section V concludes this paper.

II. THEORY OF CHARACTERISTIC MODES ANALYSIS

Basic mathematical background of CMA has been provided in [30]. From the electrical field integral equation (EFIE) of the method of moments (MoM), a complex impedance matrix can be obtained,

$$Z = R + j \cdot X \tag{1}$$

where R is the real part and X is the imaginary part. The characteristic modes can be defined as,

$$X \cdot J_n = \lambda_n \cdot R \cdot J_n \tag{2}$$

where J_n is the eigencurrents of mode order n and λ_n is the eigenvalue, ranging from $-\infty$ to $+\infty$. The induced currents on the metal body can be written as a superposition of J_n.

$$J = \sum_n \alpha_n J_n \tag{3}$$

According to boundary condition, modal coefficient α_n can be further calculated.

$$\alpha_n = \frac{V_n^i}{1 + j\lambda_n} \tag{4}$$

The numerator represents the modal excitation coefficient and the modal significance (MS) is defined in (5), ranging from 0 to 1, as a function of frequency. Modes with MS close to 0 could be ignored; Modes with MS close to 1 contribute to the induced current distribution significantly;

$$\mathrm{MS} = \left| \frac{1}{1 + j\lambda_n} \right| \tag{5}$$

Based on MS curve, we can investigate intrinsic property of each mode clearly. Spoof-LSP resonances are narrowband resonances, covering over a wide frequency span. Each spoof-LSP mode on a planar structure can be tracked by performing CMA repeatedly at sampling frequencies at will. Then, we can investigate how each spoof-LSP resonant mode evolves from non-resonant state, MS = 0, to strong resonant state, MS = 1.

Independent of any specific external sources, CMA provides a powerful method to investigate each mode at the full frequency band, and many characteristics of spoof-LSP resonances could be obtained, including eigencurrents, resonant frequencies, and bandwidths. Eigencurrents could be obtained by equation (2); MS curves reveal the resonant frequency; moreover, the half-power bandwidth (HPB) of MS curves contains the information about resonant bandwidths [29].

$$\mathrm{HPB} = \frac{f_H - f_L}{f_R} \tag{6}$$

where f_R is the center frequency of the spoof-LSP resonant mode; f_H and f_L are upper band frequency and lower band frequency, determined by half-MS value.

$$\mathrm{MS}(f_R) = 1 \tag{7}$$

$$\mathrm{MS}(f_H) = \mathrm{MS}(f_L) = \frac{1}{\sqrt{2}} \tag{8}$$

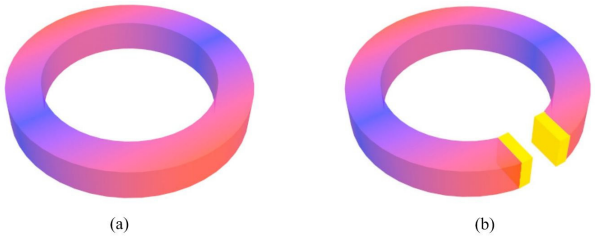

FIGURE 1. Configuration of complex spoof-LSP resonators. (a) Toroid resonator. (b) F-P type resonator.

HPBs of NF spectra or ECS spectra also contain the information about bandwidth; however, they are superposition of all modes and related to excitation, probes or plane waves. Therefore, it is difficult to define the bandwidth of each resonant mode by NFM and ECSS. We think it is more suitable to define the bandwidth of each spoof-LSP resonant mode according to HPB of MS curves, especially when spoof-LSP resonant modes are overlapped at a narrow frequency band.

III. COMPLEX SPOOF LOCALIZED SURFACE PLASMON RESONATORS

As shown in Fig. 1, complex spoof-LSP resonators could be divided into two classes: toroid resonators and F-P type resonators. Toroid resonators support bidirectional transmission of clockwise and clockwise to establish resonances. Resonant condition of the toroid resonator is written as below [12], [13]

$$k_{sp} \times C = 2\pi n \tag{9}$$

where k_{sp} is the wave vector of SSPPs, n is the mode order, C is the circumference of the toroid resonator which could also be represented as $P \times N$, the product of periodic length P and the number of unit cell N. DCA is based on this equation to calculate resonant frequencies: when the circumference and the wave vector are obtained, the resonant frequency of different modes could be calculated.

Different from the toroid resonators, F-P type resonators consist of two reflective terminals, trapping SSPPs in the wave guide between two terminals to form standing waves. Regarding the boundary condition as a new parameter to control spoof-LSP resonances, we propose complex F-P type spoof-LSP resonators with various boundary conditions, including open, shorted and reactive terminals. Taking phase shifts at two terminals into consideration, we extend the resonant condition of spoof-LSP resonances on the traditional toroid resonator to a more general situation,

$$k_{sp} \times C \times \frac{\alpha}{2\pi} + \Delta\varphi_1 + \Delta\varphi_2 = 2\pi n \tag{10}$$

α is the angle of fan-shaped textured metal region where SSPPs could propagate, phase shifts at two reflecting terminals are denoted as $\Delta\varphi_1$ and $\Delta\varphi_2$ where positive values of these numbers correspond to the inductive boundary, and negative values correspond to capacitive boundary. It is worthy to be mentioned that the traditional resonant condition in (9) could be regarded as a special condition when α is 2π, and $\Delta\varphi_1$ and $\Delta\varphi_2$ are both zero.

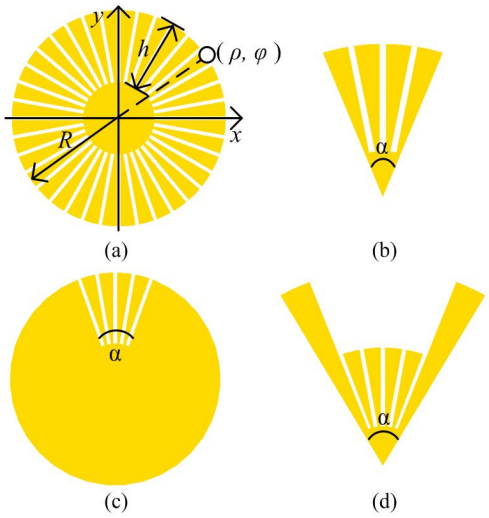

FIGURE 2. Configuration of complex spoof-LSP resonators. Conventional spoof-LSP resonator: (a) Toroid resonator. Complex F-P type spoof-LSP resonators with various boundary conditions: (b) Open-terminal; (c) Shorted-terminal; (d) Reactive-terminal.

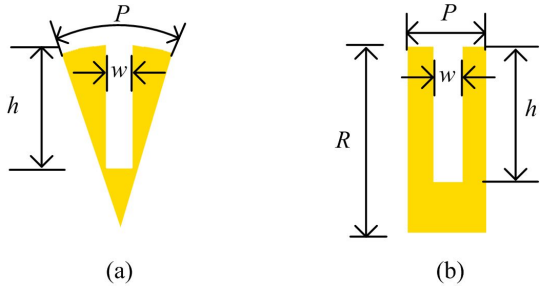

FIGURE 3. Unit cell. (a) Fan-shaped unit cell. (b) Square-shaped unit cell.

Fig. 2 shows the four complex spoof-LSP resonators under investigation. The traditional toroid resonator is shown in Fig. 2(a). The open-terminal F-P type resonator is shown in Fig. 2(b). The shorted-terminal F-P type resonator and the reactive-terminal F-P type resonator are proposed in this section to support spoof-LSP resonances. An arc metal patch is placed to connect two terminals to form the shorted terminal in Fig. 2(c). In Fig. 2(d), we design a pair of longer metal teeth on both sides of the corrugated reign to establish reactive terminals; and the shape of longer teeth outside decides the reflection phase at terminals. Fig. 3 shows detailed structures of unit cell where Fig. 3(a) shows the fan-shaped unit cell of real designs and Fig. 3(b) shows the square-shaped unit cell in simulations. Fig. 4 shows the dispersion curves of three unit cells with different groove height h. Among these lines, the black line is the dispersion curve of the unit cell under investigation in the following sections. Resonant frequencies of a traditional toroid resonator are decided by dispersion curves according to equation (10). The size of grooves affects the dispersion curve; therefore it brings shifts

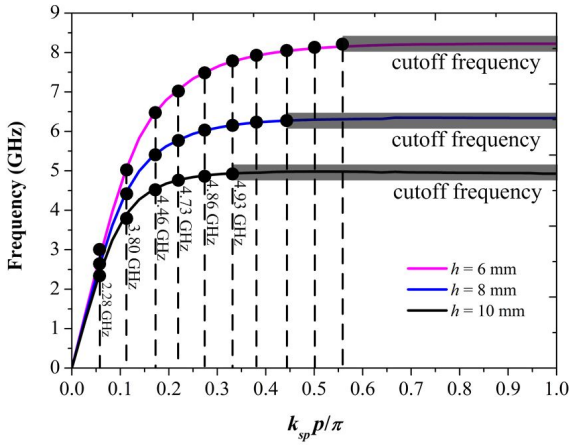

FIGURE 4. Dispersion curves (pink, blue, black lines) and resonant states (black dots) of toroid resonators with different groove heights (6 mm, 8 mm, 10 mm) and the same period length p(2.6 mm). The black line is the dispersion curve of the unit cell under investigation where six resonant frequencies on the toroid resonator are estimated by DCA (2.28 GHz, 3.80 GHz, 4.46 GHz, 4.73 GHz, 4.86 GHz and 4.93 GHz).

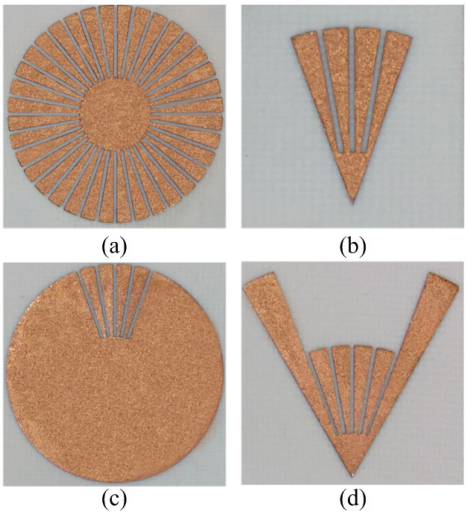

FIGURE 5. Photos of complex spoof-LSP resonators. Conventional spoof-LSP resonator: (a) Toroid resonator. Complex F-P type spoof-LSP resonators with various boundary conditions: (b) Open-terminal; (c) Shorted-terminal; (d) Reactive-terminal.

to resonant frequencies. The resonant states with stronger slow wave effect are more sensitive to the size of grooves. In addition, the cutoff frequency decides the number of resonant states and no resonant states could be found above the cutoff frequency. Photos of four resonators under investigation are shown in Fig. 5. 35 um thick copper patches with periodic grooves are supported by 508 um thick Rogers 4003C dielectric substrate. Geometric parameters of unit cells are exactly the same: the out radius R is 15 mm, the height of grooves h is 10 mm, and the width of grooves w is 0.5 mm. The length of outside teeth of reactive-terminal resonator is 25 mm.

IV. SIMULATED AND MEASURED RESULTS

In this section, several simulated and measured results of the four complex spoof-LSP resonators are presented to illustrate

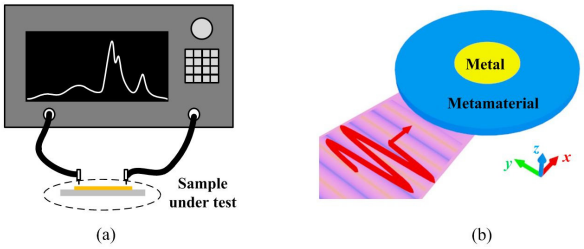

FIGURE 6. (a) The scheme to conduct NFM. (b) The scheme to conduct ECSS.

TABLE 1. CMA of spoof-LSP resonance modes.

Resonators	Mode Order	Frequency	HPB
Toroid resonator	M1	3.330 GHz	—
	M2	4.275 GHz	4.91 %
	M3	4.796 GHz	0.31 %
	M4	4.812 GHz	0.30 %
	M5	4.827 GHz	0.27 %
	M6	4.841 GHz	0.20 %
Open-terminal F-P type resonator	M1	4.743 GHz	1.60 %
	M2	4.842 GHz	1.34 %
Shorted-terminal F-P type resonator	M1	4.020 GHz	—
	M2	4.782 GHz	1.78 %
	M3	4.870 GHz	1.02 %
Reactive-terminal F-P type resonator	M1	2.630 GHz	6.65 %
	M2	4.578 GHz	1.83 %
	M3	4.818 GHz	0.37 %

the properties of CMA. The results obtained by CMA are compared to results of the conventional methods.

As shown in Fig. 6(a), NFM of spoof-LSP resonators is based on a 2-ports network analyzer; the network analyzer is connected to a pair of electric probes by two cables; the probes are placed near the spoof-LSP resonator. NF spectra of the four complex spoor-LSP resonators are tracked and resonant peaks could be observed in Fig. 7(a), (d), (g), (j). As shown in Fig. 6(b), ECS is defined as the sum of the radar cross section (RCS) and absorption cross section (ACS) to give the total monochromatic power removed from incident waves by the combined effect of scattering and absorption [31].

$$\text{ECS}=\text{ACS}+\text{RCS} \tag{11}$$

Incident linear-polarized plane waves (the magnetic vector H pointing along z direction, and the electronic vector E pointing along y direction) propagate towards the spoof-LSP resonator (along x direction); Resonant states could be excited when the frequency of incident waves is the same with the resonant frequency. Resonant peaks could be observed on the ECS spectra as shown in Fig. 7(b), (e), (h), and (k).

CMA is conducted repeatedly by solving the eigenvalue problem in (3) at each frequency sample. Fig. 7 (c), (f), (i), and (l) display MS curves and detailed results are listed in Table 1. Fig. 8, Fig. 9, Fig. 10 and Fig. 11 show

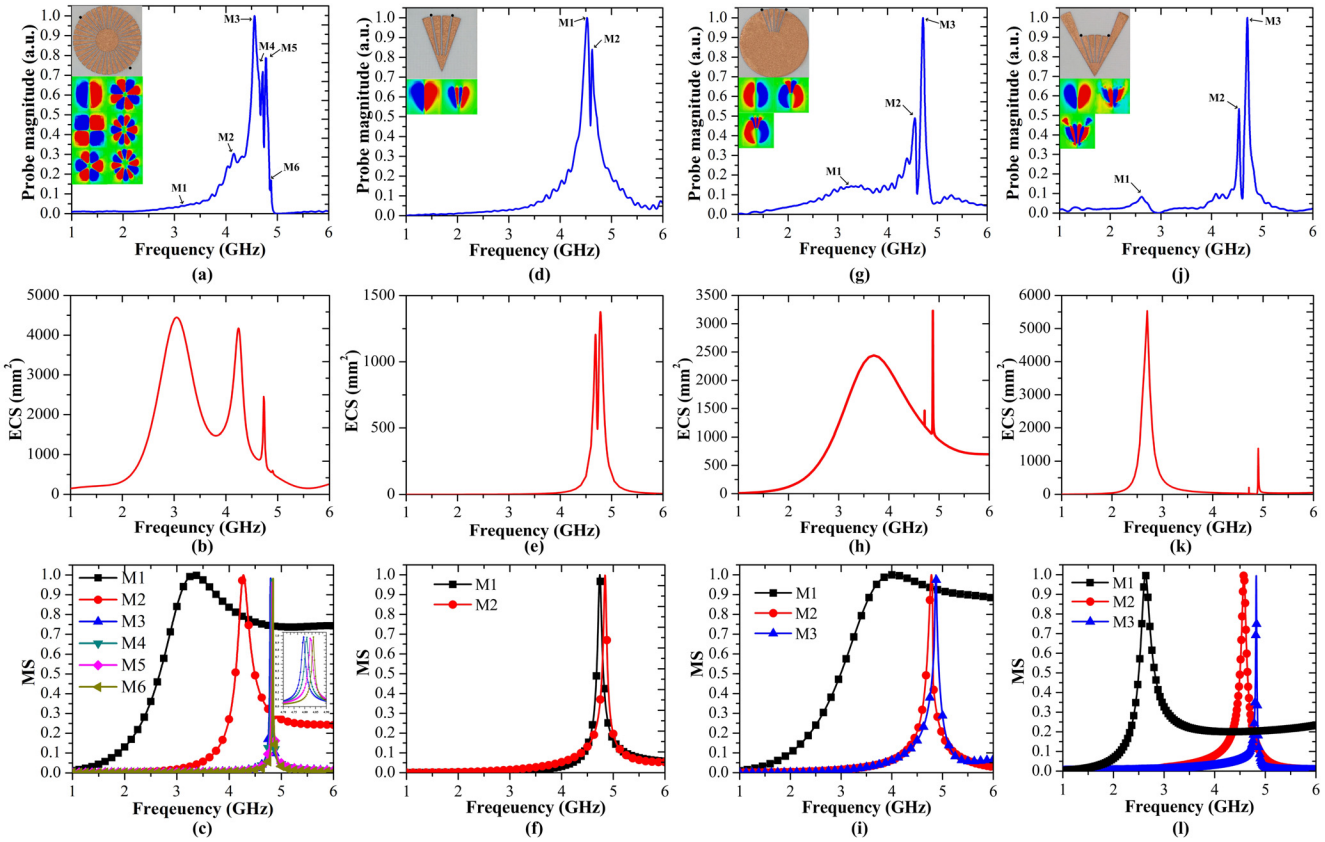

FIGURE 7. Spoof-LSP response spectra obtained by three methods, NFM, ECSS, and CMA. Inset pictures are manufactured resonators where pairs of black dots represent near field probes, electric field distribution of each resonant mode. (a) - (c) Mode spectra of toroid resonator. (d) - (f) Mode spectra of open-terminal F-P type resonator. (g) - (i) Mode spectra of shorted-terminal F-P type resonator. (j) - (k) Mode spectra of reactive-terminal F-P type resonator.

eigencurrents distribution calculated by CMA. Distribution of eigencurrents reveals resonant modes which are named in succession: Mode1 (M1), Mode2 (M2), Mode3 (M3), and so on.

Firstly, we analyze the traditional toroid resonator. The traditional toroid resonator contains 36 unit cells; therefore resonant modes exist when waves pass every unit cell with the phase shift meeting $10\times N$ degrees, DCA results are shown in Fig. 4. The six resonant modes exist below the cut off frequency and resonant frequencies are labeled. The deviations, especially at low frequency band are included inevitably due to the geometric approximation. Fig. 7(a)-(c) show response spectra. Resonant frequencies are similar; however, difference could be found because the excitations are different. The lower order modes, M1 and M2, in the NF response spectrum shown in Fig. 7(a) and higher order modes, M5 and M6, in the ECS spectrum shown in Fig. 7(b) are weakly excited; however, MS curves track the change of six resonant modes clearly as shown in Fig. 7(c). Fig. 8 shows eigencurrents distribution of the six resonant modes based on CMA respectively. Both the electric field and the eigencurrents of different resonant modes are dipole, quadrupole, hexapole, octupole, decapole, dodecapole distributed. Moreover, the MS curves also give information about the resonant bandwidth of different modes. As shown in Table 1, the higher order modes exhibit narrower bandwidth, and hence are not obtained easily from the NF spectrum and the ECS spectrum, especially when resonant modes are overlapped at a narrow band.

Secondly, we analyze the open-terminal resonator. The number of unit cells is far less than the toroid resonator; therefore, the number of resonant modes decreases dramatically. Fig. 7(d)-(f) show response spectra where two resonant peaks could be observed by different methods. It is remarkable that both two resonant peaks could be observed by NFM, ECSS and CMA. Fig. 9 shows eigencurrents distribution of two different resonant modes. Dipole and quadrupole distributions match well with electric fields. Bandwidths of different modes are shown in Table 1. Bandwidths of two modes are similar; M3 is just a little narrower than M2.

Thirdly, we analyze the shorted-terminal resonator. Fig. 7(g)-(i) show response spectra and Fig. 10 shows the eigencurrents distribution. Three resonant modes could be observed. M1 is a wideband resonant mode depending on the geometry of the metal patch; and two higher order modes, M2 and M3, are both spoof-LSP resonant modes whose resonant frequencies are almost the same as resonant frequencies of open-terminal F-P type resonators. It is compre-

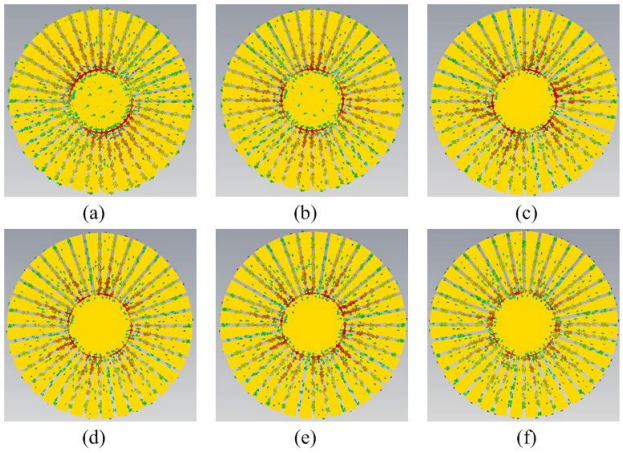

FIGURE 8. Eigencurrents distribution of resonant modes on the toroid resonator. (a) M1 (Dipole mode). (b) M2 (Quadrupole mode). (c) M3 (Hexapole mode). (d) M4 (Octopole mode). (e) M5 (Decapole mode). (f) M6 (Dodecapole mode).

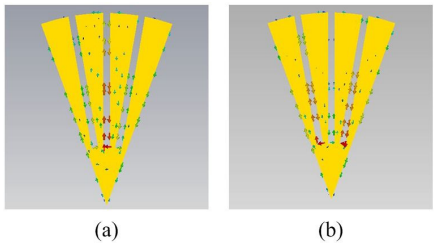

FIGURE 9. Eigencurrents distribution of resonant modes on the open-terminal F-P type resonator. (a) M1 (Dipole mode). (b) M2 (Quadrupole mode).

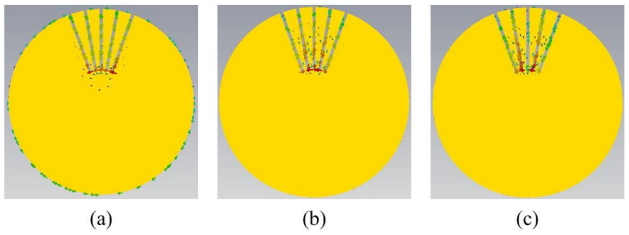

FIGURE 10. Eigencurrents of resonant modes on the shorted-terminal F-P type resonator. (a) M1 (Dipole mode). (b) M2 (Quadrupole mode). (c) M3 (Hexapole mode).

hensible because both the number and geometric parameters of grooves are exactly the same, and because total phase shifts at short-terminals and open-terminals are both 2π. M1, the ultra-wideband (UWB) radiation mode in the NF spectrum is too weak to be observed; resonant peaks of M2 are almost immersed in background scattering. However, MS curves track all the three modes. And the bandwidths of M2 and M3 are listed in Table 1.

Finally, we analyze the reactive-terminal resonator. Fig. 7(j)-(*l*) show response spectra. Three resonant modes could be found. Eigencurrents distribution of each spoof-LSP resonant mode is shown in Fig. 11. Eigencurrents

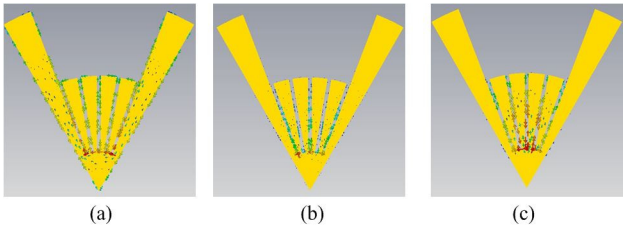

FIGURE 11. Eigencurrents distribution of resonant modes on the reactive-terminal F-P type resonator. (a) M1 (Dipole mode) (b) M2 (Quadrupole mode). (c) M3 (Hexapole mode).

of M1 distribute on the surface of outer longer teeth, while almost all eigencurrents of M2 and M3 mainly distribute on the inner corrugated region. It indicates that all resonant modes should be spoof-LSP resonant modes: M1 is supported by the pair of longer teeth on both side of corrugated region. M2 and M3 are supported by inner corrugated region whose center frequencies shift a little compared with resonant frequencies of open and shorted terminal resonators. The frequency shift is caused by phase shifts at reactive terminals. In this case, the tiny redshift indicates the pair of longer metal arms enhances the capacitance at terminals. Bandwidths of all the three modes are listed in Table 1. The higher order modes exhibit narrower bandwidth.

Resonant frequencies obtained by NFM, ECSS and CMA are similar, indicating the correctness of all these methods. However, both NFM and ECSS could not perform well at the full frequency band; NFM could not track low frequency resonance and ECSS could not track high frequency resonance. However, CMA performs well at the full frequency band; CMA tracks each resonant mode from non-resonant state to resonant state and provides eigencurrents distributions. Based on MS curve, CMA also provides a method to study the bandwidth of each resonant state. According to (6), HPBs of most resonant modes are listed in Table 1, except M1 on the toroid resonator and the shorted-terminal resonator because they are both wideband modes expanding outside the investigated frequency band.

V. CONCLUSION

Various studies of generating and detecting spoof-LSP resonances have been reported; however, more powerful methods to investigate complex spoof-LSP resonances remain untapped. We discuss CMA of complex spoof-LSP resonators in this paper, bringing CMA from the field of antenna designs to the field of surface wave resonances. Four complex spoof-LSP resonators are investigated by CMA at the full frequency band; resonant frequency, resonant bandwidth, and eigencurrents distribution are obtained. Moreover, in this paper, the concept of complex F-P type spoof-LSP resonators with various boundary conditions is fist proposed and analyzed by CMA, providing more parameters to manipulate complex spoof-LSP resonances. CMA results are compared to results obtained by NFM and ECSS; similar resonant frequencies are obtained. Therefore, we regard CMA as a powerful method to

investigate complex spoof-LSP resonances. Hopefully, CMA may have potential applications in the field of LSP at optical band.

REFERENCES

[1] R. Elliott, "On the theory of corrugated plane surfaces," *Trans. IRE Prof. Group Antennas Propag.*, vol. 2, no. 2, pp. 71–81, Apr. 1954.

[2] R. A. Hurd, "The propagation of an electromagnetic wave along an infinite corrugated surface," *Can. J. Phys.*, vol. 32, no. 12, pp. 727–734, Dec. 1954.

[3] R. Hougardy and R. Hansen, "Scanning surface wave antennas–Oblique surface waves over a corrugated conductor," *IRE Trans. Antennas Propag.*, vol. 6, no. 4, pp. 370–376, Oct. 1958.

[4] J. B. Pendry, L. Martín-Moreno, and F. J. Garcia-Vidal, "Mimicking surface plasmons with structured surfaces," *Science*, vol. 305, pp. 847–848, Aug. 2004.

[5] Barnes, L. William, A. Dereux, and T. W. Ebbesen, "Surface plasmon subwavelength optics," *Nature*, vol. 424, pp. 824–830, Aug. 2003.

[6] X. Shen, T. J. Cui, D. Martin-Cano, and F. J. Garcia-Vidal, "Conformal surface plasmons propagating on ultrathin and flexible films," *Proc. Nat. Acad. Sci. USA*, vol. 110, no. 1, pp. 40–45, Nov. 2013.

[7] H.-F. Ma, X. Shen, Q. Cheng, W. X. Jiang, and T. J. Cui, "Broadband and high-efficiency conversion from guided waves to spoof surface plasmon polaritons," *Laser Photon. Rev.*, vol. 8, no. 1, pp. 146–151, Jan. 2014.

[8] J. J. Xu, H. C. Zhang, Q. Zhang, and T. J. Cui, "Efficient conversion of surface-plasmon-like modes to spatial radiated modes," *Appl. Phys. Lett.*, vol. 106, no. 2, Jan. 2015, Art. no. 021102.

[9] A. Kianinejad, Z. N. Chen, and C.-W. Qiu, "Low-loss spoof surface plasmon slow-wave transmission lines with compact transition and high isolation," *IEEE Trans. Microw. Theory Techn.*, vol. 64, no. 10, pp. 3078–3086, Oct. 2016.

[10] Z. Xu, S. Li, X. Yin, H. Zhao, and L. Liu, "Radiation loss of planar surface plasmon polaritons transmission lines at microwave frequencies," *Sci. Rep.*, vol. 7, Jul. 2017, Art. no. 6098.

[11] A. Pors, E. Moreno, L. Martin-Moreno, J. B. Pendry, and F. J. Garcia-Vidal, "Localized spoof plasmons arise while texturing closed surfaces," *Phys. Rev. Lett.*, vol. 108, no. 22, Jun. 2012, Art. no. 223905.

[12] X. Shen and T. J. Cui, "Ultrathin plasmonic metamaterial for spoof localized surface plasmons," *Laser Photon. Rev.*, vol. 8, no. 1, pp. 137–145, Nov. 2013.

[13] Z. Gao, F. Gao, H. Xu, Y. Zhang, and B. Zhang, "Localized spoof surface plasmons in textured open metal surfaces," *Opt. Lett.*, vol. 41, no. 10, pp. 2181–2184, May 2016.

[14] Z. Gao, F. Gao, Y. Zhang, H. Xu, Y. Luo, and B. Zhang, "Forward/backward switching of plasmonic wave propagation using sign-reversal coupling," *Adv. Mater.*, vol. 29, no. 26, Jul. 2017, Art. no. 1700018.

[15] H.-W. Wu, H.-J. Chen, H.-Y. Fan, Y. Li, and X.-W. Fang, "Trapped spoof surface plasmons with structured defects in textured closed surfaces," *Opt. Lett.*, vol. 42, no. 4, pp. 791–794, Feb. 2017.

[16] P. A. Huidobro *et al.*, "Magnetic localized surface plasmons," *Phys. Rev. X*, vol. 4, no. 2, Apr. 2014, Art. no. 021003.

[17] Y. Lan, "Multipole Modes excitation of uncoupled dark plasmons resonators based on frequency selective surface at X-band frequency regime," *Sci. Rep.*, vol. 7, Dec. 2017, Art. no. 9492.

[18] D. Bao, K. Z. Rajab, W. X. Jiang, Q. Cheng, Z. Liao, and T. J. Cui, "Experimental demonstration of compact spoof localized surface plasmons," *Opt. Lett.*, vol. 41, no. 23, pp. 5418–5421, Dec. 2016.

[19] Y. J. Zhou, Q. X. Xiao, and B. J. Yang, "Spoof localized surface plasmons on ultrathin textured MIM ring resonator with enhanced resonances," *Sci. Rep.*, vol. 5, Sep. 2015, Art. no. 14819.

[20] K. Fujita, "A partially implicit FDTD method for the wideband analysis of spoof localized surface plasmons," *IEEE Photon. Technol. Lett.*, vol. 27, no. 10, pp. 1124–1127, May 15, 2015.

[21] B. Luk'yanchuk *et al.*, "The Fano resonance in plasmonic nanostructures and metamaterials," *Nature Mater.*, vol. 9, no. 9, pp. 707–715, Aug. 2010.

[22] N. A. Mirin, K. Bao, and P. Nordlander, "Fano resonances in plasmonic nanoparticle aggregates," *J. Phys. Chem. A*, vol. 113, no. 16, pp. 4028–4034, Jan. 2009.

[23] R. J. Garbacz and R. Turpin, "A generalized expansion for radiated and scattered fields," *IEEE Trans. Antennas Propag.*, vol. AP-19, no. 3, pp. 348–358, May 1971.

[24] Q. Wu, W. Su, Z. Li, and D. Su, "Reduction in out-of-band antenna coupling using characteristic mode analysis," *IEEE Trans. Antennas Propag.*, vol. 64, no. 7, pp. 2732–2742, Jul. 2016.

[25] C. Li and R. Mittra, "Controlling radiation patterns of antennas mounted on complex platforms using the characteristic basis functions (CBFs)," *J. Electromagn. Appl.*, vol. 30, no. 10, pp. 1354–1365, May 2016.

[26] A. A. Salih, Z. N. Chen, and K. Mouthaan, "Characteristic mode analysis and metasurface- based suppression of higher order modes of a 2×2 closely spaced phased array," *IEEE Trans. Antennas Propag.*, vol. 65, no. 3, pp. 1141–1150, Mar. 2017.

[27] F. H. Lin and Z. N. Chen, "Low-profile wideband metasurface antennas using characteristic mode analysis," *IEEE Trans. Antennas Propag.*, vol. 65, no. 4, pp. 1706–1713, Apr. 2017.

[28] P. Ylä-Oijala, D. C. Tzarouchis, E. Raninen, and A. Sihvola, "Characteristic mode analysis of plasmonic nanoantennas," *IEEE Trans. Antennas Propag.*, vol. 65, no. 5, pp. 2165–2172, May 2017.

[29] Y. Chen and C.-F. Wang, *Characteristic Modes: Theory and Applications in Antenna Engineering*. Hoboken, NJ, USA: Wiley, 2015.

[30] M. Vogel, G. Gampala, D. Ludick, U. Jakobus, and C. J. Reddy, "Characteristic mode analysis: Putting physics back into simulation," *IEEE Antennas Propag. Mag.*, vol. 57, no. 2, pp. 307–317, Apr. 2015.

[31] M. I. Mishchenko, L. D. Travis, and A. A. Lacis, *Scattering, Absorption, and Emission of Light by Small Particles*. Cambridge, U.K.: Cambridge Univ. Press, 2002.

ZHIXIA XU (S'15) was born in Wuxi, China. He received the B.Eng. degree in electronic information science and technology from Dalian Maritime University, Dalian, China, in 2015. He is currently pursuing the Ph.D. degree in electromagnetic field and microwave technique with Southeast University, Nanjing, China. His current research interests include antenna theory and designs, periodic structures, and surface waves.

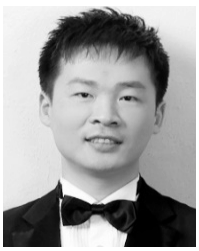

SHUNLI LI (S'10–M'15) was born in Liaocheng, Shandong, China, in 1984. He received the B.S. degree in science and technology of electronic information and the M.S. degree in radio physics from Shandong University, in 2007 and 2010, respectively, and the Ph.D. degree in electromagnetic field and microwave technology from the State Key Laboratory of Millimeter Waves, Southeast University (SEU), in 2015. In 2015, he joined the Department of Electrical and Computer Engineering, National University of Singapore, as a Research Fellow. In 2017, he joined the State Key Laboratory of Millimeter Waves, SEU, with interests in ultrawideband antennas and arrays, time-domain analysis, microwave passive devices, and short-pulse antennas and networks.

YANQUN LIU (S'14) was born in Kaifeng, Henan, China, in 1991. He received the B.Eng. degree in information engineering from the School of Information Science and Engineering, Southeast University, Nanjing, China, in 2014, where he is currently pursuing the Ph.D. degree in antenna and propagation.

HONGXIN ZHAO (M'11) was born in Hongze, Jiangsu, China, in 1971. He received the B.S.E. degree in radio communication techniques and the Ph.D. degree in microwave techniques from Southeast University, Nanjing, China, in 1993 and 2003, respectively. In 1996, he joined the Research Team, State Key Laboratory of Millimeter Waves, Southeast University, with interest in microwave circuit design. He is interested in the research of signal processing and control.

XIAOXING YIN (M'03) was born in Taiyuan, China. He received the B.Sc. degree in radio engineering and the M.Sc. and Ph.D. degrees in electrical engineering from Southeast University, Nanjing, China, in 1983, 1989, and 2001, respectively. During 1983–1986 and 1989–1998, he was with the Department of Physics, University of Petroleum, Dongying, China, where he conducted research in the areas of logging methods and instruments. Since 2001, he has been a Lecturer with the State Key Laboratory of Millimeter Waves, Southeast University, where he is currently a Professor. His current research interests include computational electromagnetics, microwave passive circuit components, and antennas.